Compact Design of a L-Band 40W 40MHz Envelope Tracking GaN Power Amplifier for Small Cells

Olivier Nonet, Wilfried Demenitroux, Frederic Ploneis, Denis Barataud, Michel Campovecchio

Compact Design of a L-Band 40W 40MHz Envelope Tracking GaN Power Amplifier for Small Cells

Olivier Nonet[#*], Wilfried Demenitroux[#], Frederic Ploneis[#], Denis Barataud[*], Michel Campovecchio[*]

[#]Thales SIX GTS, France

[*]XLIM, UMR CNRS-7252, Université de Limoges, France

{olivier.nonet, denis.barataud, michel.campovecchio}@xlim.fr, {wilfried.demenitroux, frederic.ploneis}@thalesgroup.com

***Abstract*— Envelope Tracking (ET) greatly enhances the efficiency of High Power Amplifiers (HPA) driven by modulated signals associated with high Peak-to-Average Power Ratio (PAPR) and high bandwidth schemes. This paper presents a 40 W compact plastic-packaged GaN MMIC HPA connected to its integrated GaN MMIC Supply Modulator (SM). The whole ET-PA design fits in 25 cm^2 and demonstrates an efficiency improvement greater than 25 points for the selected modulation schemes with PAPR in the 4-6.5 dB range. When compared to constant DC bias conditions, the ET system reduces the thermal dissipation by 50%, thus making such a compact integration possible within the safe operating area. The ET-PA system can be used for any high-PAPR radio application as its compactness facilitates the integration into smart cells belonging to phased-array networks or modern base transceiver stations.**

***Keywords*— Envelope Tracking, High-efficiency Power Amplifier, GaN, plastic QFN, DC/DC Supply Modulator, small cells.**

I. Introduction

Power amplifiers (PA) account for most of the overall current consumption in modern communication systems. Today, high PAPRs caused by orthogonal frequency-division multiplexing (OFDM) signals drastically limit the performances of HPA, leading to inadequate conventional architectures.

Envelope Tracking (ET) is a powerful technique to enhance efficiency in high instantaneous bandwidth modulations and high-PAPR schemes [1]. The supply modulator (SM) keeps the HPA saturated at high efficiency levels most of the time. In line with the SWaP-C principle (i.e Size, Weight, Power, and Cost), the major advantages of ET are smaller consumption, better thermal management, and cost-effective usage of components. For small cell applications, the HPA needs to be as small and low-cost as possible. In this regard, the ET architecture is mandatory for dramatically reducing the power dissipation, thus allowing the design of QFN-packaged (Quad Flat No Leads) HPAs.

This paper proposes the compact design of a plastic-packaged 40 W GaN MMIC HPA connected to a GaN MMIC supply modulator. Section II presents the architecture of the ET-PA system. Sections III outlines and discusses the results of both the ET and fixed-bias configurations. Section IV draws conclusions and gives perspectives about future work.

II. Building Blocks of the ET-PA Design

The designed and fabricated ET-PA system integrated in a test bench is presented in Fig. 1 with its three fundamental building blocks, namely the supply modulator, the RF HPA, and the averaging low-pass output filter. The test bench is used to characterize the ET-PA in terms of average powers and envelope currents, voltages and powers.

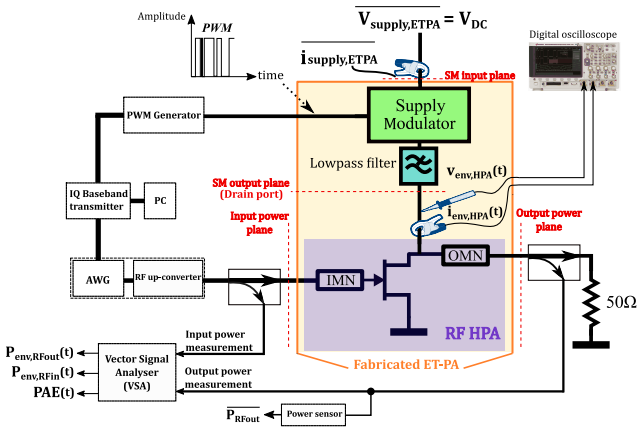

Fig. 1. ET-PA block diagram and its associated measurement setups.

$$\overline{P_{supply,ETPA}} = \overline{i_{supply,ETPA(t)}} \times V_{DC} \quad (1)$$

$$\overline{P_{supply,HPA}} = \frac{1}{T_{env}} \int_0^{T_{env}} i_{env,HPA(t)}.v_{env,HPA(t)}.\mathrm{d}t \quad (2)$$

$$\overline{P_{dissipated,HPA}} = \overline{P_{supply,HPA}} - \overline{P_{RFout}} \quad (3)$$

$$\overline{P_{dissipated,ETPA}} = \overline{P_{supply,ETPA}} - \overline{P_{RFout}} \quad (4)$$

$$\eta_{SM} = \frac{P_{supply,HPA}}{P_{supply,ETPA}} \quad (5)$$

A. High efficiency DC/DC Supply Modulator

The DC/DC supply modulator has been designed and manufactured according to our in-house patented architecture [2], [3] using the UMS GH25 0.25 µm AlGaN/GaN commercial process. It is packaged into a 3x3mm compact low-cost plastic QFN package and has a maximum available peak output power of 50 W. The supply modulator is driven by a Pulse Width

Modulation (PWM) waveform to encode the generated analog envelope signal. Fig. 2 presents the schematic diagram of the supply modulator, which is a half-bridge configuration composed of the patented switching cell in [2].

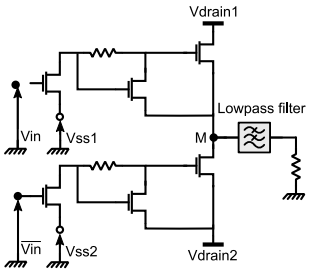

Fig. 2. Architecture of the patented supply modulator [2],[3].

Fig. 3 shows the measured efficiency defined in equation (5) of the supply modulator at a 80 MHz switching frequency versus the power Output Back-Off (OBO) for 64-QAM signals with different modulation speeds. When the OBO reaches its maximum value, the supply modulator works at its highest efficiency. This characteristic crucially compensates for the degraded efficiency of the HPA at high OBO values.

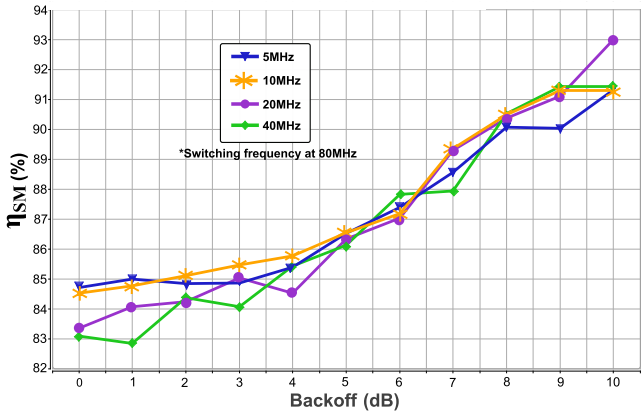

Fig. 3. Supply Modulator efficiency (%) vs. OBO (dB) for 64-QAM signals at different modulation speeds for a 80 MHz switching frequency.

B. MMIC RF Power Amplifier

To eliminate costly and time-consuming development processes, a commercial low-cost 40 W GaN MMIC HPA integrated into a 5x5 mm QFN plastic package has been selected. The peak RF output power at 50 V drain bias is rated at 46 dBm with 60% Power Added Efficiency (PAE) and 27 dB power gain in the 0.9-1.7 GHz band.

As the HPA is QFN-packaged, the design of the ET-PA environment had to carefully address the delicate issue of thermal management. In this regard, the ET solution was implemented through the design of the required DC/DC converter to offer a significant reduction in DC consumption for a wide range of output powers and for wideband modulation schemes. As shown in the next section, the manufactured ET system provides a decisive improvement in the thermal behavior within the safe-operating area to allow QFN packaging.

C. Output filter design

The low-pass filter connects the output of the supply modulator to the drain bias port of the MMIC HPA (Fig. 1) and plays a critical role in rejecting the switching frequency and its associated even recombinations. The bandwidth of the filter is 50 MHz to ensure low-loss transmissions of the dynamic drain signals up to a maximum speed of 40 MHz. However, the dynamic drain bias of the ET-PA means, in fact, that the drain load impedance is no longer constant since it depends on the instantaneous current driven by the HPA. This drawback of ET-PA deteriorates the filter characteristics by modifying its frequency response and drain signals. To overcome this issue, we designed a Legendre-Papoulis filter providing a trade-off between the group delay and the stopband attenuation [4].

D. Implementation of the ET-PA

All previous elements have been implemented on a 4-layer board, which is presented in Fig. 4. To meet the requirements of RF power and efficiency trajectory, a polynomial bias law has been calculated at each RF input power level which dynamically supplies the right drain voltage value to the HPA.

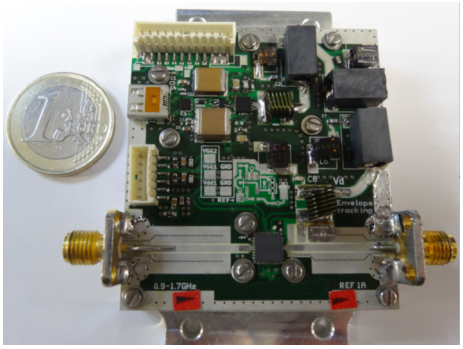

Fig. 4. Stand-alone ET-PA system including the SM and the RF HPA.

In such a way, the ET system keeps the PAE as high as possible at the highest OBO while meeting the RF output power requirements. No Digital Pre-Distortion (DPD) has been applied in our measurement due to instrument limitations.

III. Experimental Results

This section compares the measured results of three distinct modulation schemes with a carrier frequency in the 1.3-1.5 GHz range for both the ET (15-45 V) and the fixed-bias (45 V) configurations. The average power consumption of the HPA is presented in Fig. 5 for a 64-QAM modulated signal with a 40 MHz modulation bandwidth.

Fig. 5 shows that ET gives from 4 W up to 7 W of reduction in consumption (i.e. 50%) over a large RF dynamic range. Fig. 6 highlights the thermal improvement provided by the ET in both cases of a 64-QAM 40 MHz and a QPSK 2 MHz modulation associated with a smaller PAPR scenario. The green area in Fig. 6 shows that the thermal dissipation decreases by 56% (-6.5 W) at 36 dBm output power for the 40 MHz 64-QAM modulation.

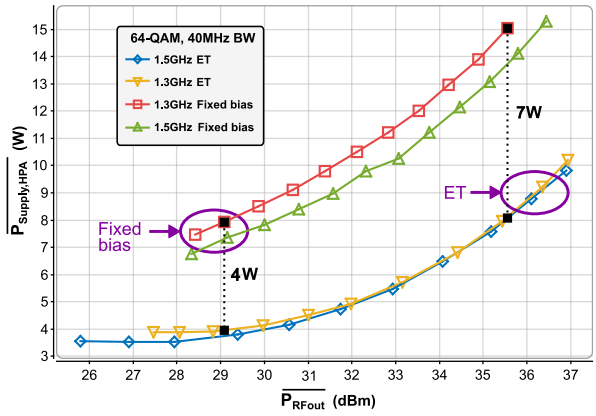

Fig. 5. Average supply consumption of the HPA ($\overline{P_{supply,HPA}}$) versus the average RF output power ($\overline{P_{RFout}}$). Comparison between ET-PA (Supply Modulator activated) and fixed bias HPA (no SM).

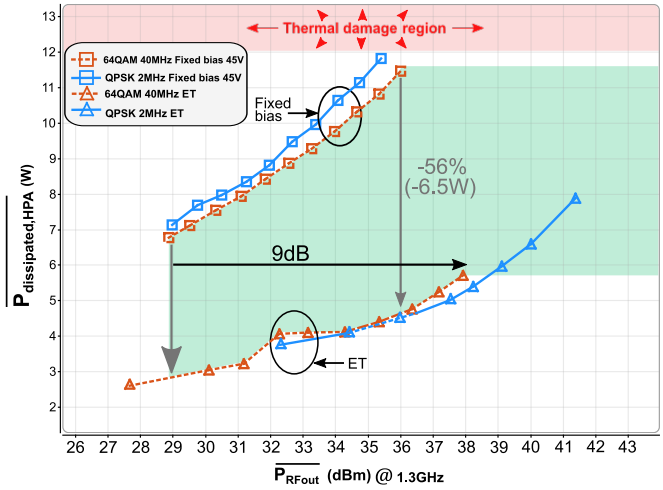

Fig. 6. HPA thermal dissipation ($\overline{P_{dissipated,HPA}}$) versus the average RF output power ($\overline{P_{RFout}}$). Comparison between ET-PA and fixed-bias HPA at 1.3 GHz.

Moreover, the ET increases by more than 5 dB the safe power range of the QPSK, which was initially prevented by thermal constraints. For the same amount of dissipated power by the HPA itself, the output power of the demonstrator is improved by a factor of 9 dB for the 64-QAM, and 13 dB for the QPSK. This shows the ET-PA's capability of operating under different modulation PAPR and bandwidths.

Fig. 7 presents the measured instantaneous PAE of a 64-QAM, 20 MHz, 6.5 dB PAPR signal at 1.3 GHz for both the ET and the fixed-bias configurations. The ET drain voltage operates from 15 V to 45 V whereas the fixed-bias drain voltage is 45 V. The HPA reaches 44 dBm of RF saturated output power in both configurations, corresponding to a peak PAE of 65%.

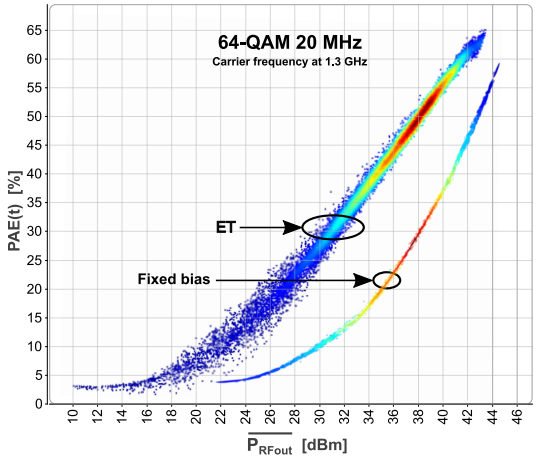

Fig. 7. Instantaneous measured PAE versus $\overline{P_{RFout}}$ of a 64-QAM 20 MHz signal for ET and fixed-bias configurations

Conversely, while the average operating efficiency of the ET-PA is around 53%, the fixed-bias configuration operates at approximately 28%, resulting in 25 points of PAE improvement. The measured output spectrum for a 64-QAM 20 MHz at 1.3 GHz is presented in Fig. 8 with 34 dBc ACPR without DPD.

Table 1 compares measurement results at three frequencies in L-band to emphasize the RF bandwidth characteristics in both fixed-bias and ET configurations. The tracking voltage

Table 1. Synthesis of the measured average output power results for three modulation schemes, in ET and fixed-bias scenarios without DPD.

Input signal		Power and linearity measurements			ET-PA (HPA+SM) DC consumption	DC supply consumption (@HPA level) $\overline{P_{supply,HPA}}$		Power improvement of ET-PA vs fixed bias		Thermal improvement of ET-PA vs fixed bias (@HPA level)	
Mod. Scheme [PAPR dB]	Freq. [GHz]	Pout [dBm]	EVM [%]	ACLR [dBc]	$\overline{P_{supply,ETPA}}$ [W] Column(A)	Fixed-bias [W] Column (B)	ET [W] Column (C)	ET-PA (HPA alone) reduction in dissipation Column (C) - Column (B)	ET-PA (HPA+SM) Reduction in DC supply consumption Column (B) - Column (A)	Fixed-bias [W]	ET [W]
QPSK 2MHz [4dB]	1.3	40	3.2	30	19.5	29.5	16.5	-13W / -67%	-10W / -34%	19.5	6.5
	1.4	40	3.4	31.5	21	31.5	16.5	-15W / -70%	-10,5W / -33%	21.5	6.5
	1.5	40	3.5	32.5	21	31.5	17.5	-14W / -65%	-10,5W / -33%	21.5	7.5
64-QAM 20MHz [6.5dB]	1.3	37	3.6	33.5	11	16	9	-7W / -64%	-5W / -31%	11	4
	1.4	37	3.7	34.5	11.5	16	9.7	-6,3W / -57%	-4,5W / -28%	11	4.7
	1.5	37	3.8	35.5	11.5	16	9.8	-6,2W / -56%	-4,5W / -28%	11	4.8
64-QAM 40MHz [6.5dB]	1.3	36	3.9	36.5	10	15.5	8.5	-7W / -61%	-5,5W / -35%	11.5	4.5
	1.4	36	4	37.5	10	14	8.5	-5,5W / -55%	-4W / -29%	10	4.5
	1.5	36	4.1	38.5	10	14.5	8.5	-6W / -57%	-4,5W / -31%	10.5	4.5

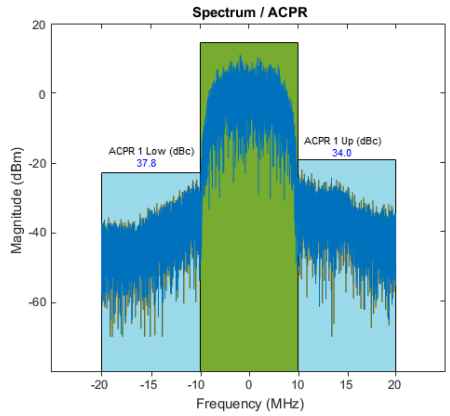

Fig. 8. Spectrum without DPD of a 64-QAM 20 MHz signal at 1.3 GHz.

generated by the SM operates in the 15 V to 45 V range. The ET-PA system integrates voltage and current measurement probes at the SM input and drain ports. Using the previous equations, we determined the average DC consumption of the ET-PA and HPA.

Indeed, equation (4) allowed us to determine the thermal improvement provided by ET in terms of dissipated power at the HPA level in ET configuration.

As demonstrated in Table 1, the ET eliminates the thermal issue of the HPA for smaller PAPR modulation schemes with a reduction in dissipated power of 65% up to 70% for the QPSK, allowing larger RF output powers and a QFN-based design.

According to the carrier frequency, the modulation scheme and bandwidth, the improvements of the ET demonstrated in Table 1 can be summarized and quantified by a reduction of 28% to 35% in DC consumption at the ET-PA system level and a reduction of 55% to 70% in thermal dissipation at HPA circuit level.

Table 2 displays the comparison between state-of-the-art performances of eight ET-PAs.

Table 2. Comparison of the performances of several state-of-the-art ET-PAs.

Ref.	Input signal			Measurement results			
	Freq. [GHz]	Mod. BW [MHz]	PAPR [dB]	Pout [dBm]	Gain [dB]	Glob. efficiency [%]	ACLR1 [dBc]
[5]	0.7-2.1	20	6.5	29.2-33	11.1-7.8	20-39	34
[6]	3.6-4.0	20	6.5	31.2-31.5	12.3-13.6	39.5-46.8	44.5-49.8
[7]	3.5	60	10	32.3	-	38.7	47
[8]	9.57	20	11.4	29.3	22	32	33
[9]	0.9-2.15	80	6.5	30-30.7	15.0-18.2	32.1-35.5	45
[10]	1.84	10	11.65	32.8	12.8	23.9	37.8
[11]	2.62-2.69	2*10	6.5	46	15	60	49
[12]	4.4-5.0	1.25	6.5	33	16-7	45-65*	44
[this work]	1.3-1.5	40	6.5	36	22	43	37.8

*These authors measured the performances without accounting for the supply modulator.

Compared to other ET-PAs, our demonstrator offers one of the highest global efficiencies and output powers along with the smallest size and QFN packaging for small cell applications.

IV. Conclusion

This paper presents a highly compact ET-PA system based on an optimized GaN MMIC supply modulator connected to a low-cost plastic-packaged QFN HPA. Such an ET-PA demonstrates an increase higher than 25 points in terms of efficiency. It means that the overall efficiency is significantly improved due to a lower consumption of all considered scenarios in terms of frequency and modulation schemes up to 6.5 dB of PAPR. In turn, the power dissipation is divided by three, keeping the HPA within the safe-operating area and allowing the use of low-cost QFN packages on conventional multilayer stack-ups. By reducing the power dissipation, this ET-PA enhances the transmitter's output power by a factor of 4 (6 dB) for a QPSK modulation, compared to the fixed-bias HPA configuration.

As the low-pass filter between SM and HPA approximately accounts for 30% of the overall PCB surface, future research should focus on the techniques to reduce its size. Amidst all investigated solutions to achieve this goal, the use of a higher switching frequency for the supply modulator seems to be one of the most promising options.

References

[1] Z. Popovic, "Amping Up the PA for 5G: Efficient GaN Power Amplifiers with Dynamic Supplies," in IEEE Microwave Magazine, vol. 18, no. 3, pp. 137-149, May 2017.

[2] O. Jardel, R. Quere, S. Piotrowicz, P. Bouysse, S. Delage, A. Martin, "Power switching cell with normally conducting field-effect transistors" Patent WO2015162063A1, Apr. 22, 2014.

[3] W. Demenitroux, L. Mandica, D. Albert, "RF radio frequency transmitter architecture" Patent WO2020016305 , Jan. 23, 2020.

[4] Z. Wang, "Envelope Tracking Power Amplifiers for Wireless Communications", Artech, 2014.

[5] T. Fujiwara et al., "All gallium nitride envelope-tracking multiband power amplifier using 200MHz switching buck-converter," 2016 11th European Microwave Integrated Circuits Conference (EuMIC), London, UK, 2016, pp. 125-128.

[6] Y. Komatsuzaki et al., "A High Efficiency 3.6-4.0 GHz Envelope-Tracking Power Amplifier Using GaN Soft-Switching Buck-Converter," 2018 IEEE/MTT-S International Microwave Symposium - IMS, Philadelphia, PA, USA, 2018, pp. 465-468.

[7] D. Fishler, T. Cappello, W. Hallberg, T. W. Barton and Z. Popovic, "Supply Modulation of a Linear Doherty Power Amplifier," 2018 48th European Microwave Conference (EuMC), Madrid, Spain, 2018, pp. 519-522, doi: 10.23919/EuMC.2018.8541618.

[8] T. Cappello, C. Florian, D. Niessen, R. P. Paganelli, S. Schafer and Z. Popovic, "Efficient X-Band Transmitter With Integrated GaN Power Amplifier and Supply Modulator," in IEEE Transactions on Microwave Theory and Techniques, vol. 67, no. 4, pp. 1601-1614, April 2019.

[9] S. Sakata et al., "An 80MHz modulation bandwidth high efficiency multi-band envelope-tracking power amplifier using GaN single-phase buck-converter," 2017 IEEE MTT-S International Microwave Symposium (IMS), Honolulu, HI, USA, 2017, pp. 1854-1857.

[10] H. Tango, T. Hashinaga, K. Totani, H. Kuriyama, Y. Hamada and T. Asaina, "A 60% efficient envelope tracking power amplifier for 40W, 2.6GHz LTE base station with in/output harmonic tuning," 2013 IEEE MTT-S International Microwave Symposium Digest (MTT), Seattle, WA, USA, 2013, pp. 1-4.

[11] W. Demenitroux, A. Thorinius, L. Mandica, F. Ploneis and N. Berthou, "New Class-F High Efficiency Multi-bias Optimised GaN HPA for C-band Applications," 2018 48th European Microwave Conference (EuMC), Madrid, Spain, 2018, pp. 344-347.